

# 11

---

## *Weighted Spherical Harmonic Representation*

---

There is a lack of a unified statistical modeling framework for cerebral shape asymmetry analysis in the literature. Most previous approaches start with flipping the 3D magnetic resonance images (MRI). The anatomical correspondence across the hemispheres is then established by registering the original image to the flipped image. A difference of an anatomical index between these two images is used as a measure of cerebral asymmetry. We present a radically different asymmetry analysis that utilizes a novel weighted spherical harmonic representation of cortical surfaces. The weighted spherical harmonic representation is a surface smoothing technique given explicitly as a weighted linear combination of spherical harmonics. This new representation is used to parameterize cortical surfaces, establish the hemispheric correspondence, and normalize cortical surfaces in a unified mathematical framework. The methodology has been applied in characterizing the cortical asymmetry of a group of autistic subjects. This chapter is mainly based on [73].

---

### **11.1 Introduction**

Previous neuroanatomical studies have shown left occipital and right frontal lobe asymmetry, and left planum temporal asymmetry in normal controls [25, 200]. These studies mainly flip the whole brain 3D MRI to obtain the mirror reflected MRI with respect to the mid-saggital cross-section. Then the anatomical correspondence across the hemispheres is established and a subsequent statistical analysis is performed at each voxel in the 3D MRI. Although this approach is sufficient for the voxel-based morphometry [14, 15], where we only need an approximate alignment of corresponding brain substructures, it may fail to properly align highly convoluted sulcal and gyral foldings of gray matter. In order to address this shortcoming inherent in 3D whole brain volume asymmetry analysis, we need a new 2D cortical surface based framework.

The human cerebral cortex has the topology of a 2D highly convoluted grey matter shell with an average thickness of 3mm. The outer boundary of the shell is called the *outer cortical surface* while the inner boundary is called the *inner cortical surface*. Cortical surfaces are segmented from magnetic resonance images (MRI) using a deformable surface algorithm and represented

as a triangle mesh consisting of more than 40,000 vertices and 80,000 triangle elements [83, 237]. Once we obtain both the outer and inner cortical surfaces of a subject, *cortical thickness*, which is the distance between the outer and inner surfaces, is computed at each vertex of the outer surface [237]. Since different clinical populations are expected to show different patterns of cortical thickness variations, cortical thickness has been used as a quantitative index for characterizing a clinical population [76]. Cortical thickness varies locally by region and is likely to be influenced by aging, development and disease [26]. By analyzing how cortical thickness differs locally in a clinical population with respect to a normal population, neuroscientists can locate the regions of abnormal anatomical differences in the clinical population. Cortical thickness serves as a metric of interest in performing 2D cortical asymmetry analysis. However, there are various methodological issues associated with using triangle mesh data. Our novel 2D surface modeling framework called the *weighted spherical harmonic representation* [71] can address these issues in a unified mathematical framework.

Cortical surface mesh construction and cortical thickness computation are expected to introduce noise. To counteract this, surface-based data smoothing is necessary. For 3D whole brain volume-based method, Gaussian kernel smoothing, which weights neighboring observations according to their 3D Euclidean distance, has been used. However, for data that lie on a 2D surface, smoothing must be weighted according to the geodesic distance along the surface [10, 83]. It will be shown that the weighted spherical harmonic representation is a 2D surface-based smoothing technique, where the explicit basis function expansion is used to smooth out noisy cortical surface data. The basis function expansion corresponds to the solution of isotropic heat diffusion. Unlike the previous surface based smoothing that solves the heat equation nonparametrically [10, 83, 76], the result of the weighted spherical harmonic representation is explicitly given as a weighted linear combination of spherical harmonics. This provides a more natural statistical modeling framework. A validation study showing the improved performance of the weighted spherical harmonic representation over heat kernel smoothing was given in [76].

Comparing measurements defined at mesh vertices across different cortical surfaces is not a trivial task due to the fact no two cortical surfaces are identically shaped. In comparing measurements across different 3D whole brain images, 3D volume-based image registration is needed. However, 3D image registration techniques tend to misalign sulcal and gyral folding patterns of the cortex. Hence, 2D surface-based registration is needed in order to compare measurements across different cortical surfaces. Various surface registration methods have been proposed before [76, 363, 99, 248, 121]. These methods solve a complicated optimization problem of minimizing the measure of discrepancy between two surfaces. Unlike the previous computationally intensive methods, the weighted spherical harmonic representation provides a simple way of establishing surface correspondence between two surfaces in reducing

the improper alignment of sulcal folding patterns without time consuming numerical optimization.

Once we establish surface correspondence between two surfaces, we also need to establish hemispheric correspondence within a subject for asymmetry analysis. However, it is not straightforward to establish a 2D surface-based hemispheric correspondence. Although there are many 3D volume-based brain hemisphere asymmetry analyses [25, 200], due to this simple reason, there is a lack of 2D surface-based asymmetry analyses. This will be the first unified mathematical framework on 2D cortical asymmetry. The inherent angular symmetry presented in the weighted spherical harmonic representation can be used to establish the inter-hemispheric correspondence. It turns out that the usual asymmetry index of  $(L-R)/(L+R)$  is expressed as the ratio between the sum of positive and negative order harmonics.

The novelty of our proposed method is that surface parameterization, surface-based smoothing, and within- and between- subject surface registration can be performed within a single unified mathematical framework that provides a more consistent modeling framework than previously available for cortical analysis.

## 11.2 Spherical Coordinates

Cortical thickness is measured at each vertex and used as a measure for characterizing cortical shape variation. There exists a bijective mapping between the cortical surface  $\mathcal{M}$  and a unit sphere  $S^2$  that is obtained via the deformable surface algorithm. Consider the parameterization of the unit sphere  $S^2$  given by

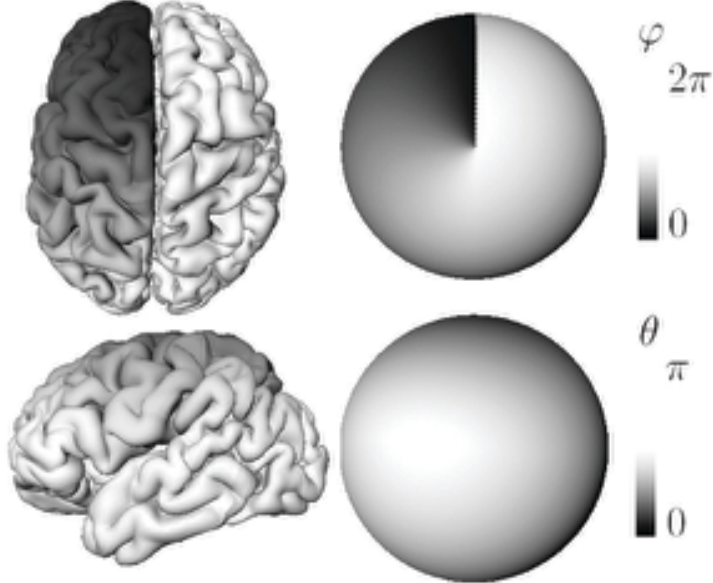
$$(u_1, u_2, u_3) = (\sin \theta \cos \varphi, \sin \theta \sin \varphi, \cos \theta),$$

with  $(\theta, \varphi) \in [0, \pi] \otimes [0, 2\pi]$ . The polar angle  $\theta$  is the angle from the north pole and the azimuthal angle  $\varphi$  is the angle along the horizontal cross-section. Then, using the bijective mapping, we can parameterize the Cartesian coordinates  $v = (v_1, v_2, v_3)$  of each cortical mesh vertex in the cortical surface  $\mathcal{M}$  with the spherical angles  $(\theta, \varphi)$ , i.e.,  $v = v(\theta, \varphi)$  (Figure 11.1). This enables us to represent cortical thickness measurements  $f$  with respect to the spherical coordinates, i.e.,  $f = f(\theta, \varphi)$ . Each component of surface coordinates will be modeled independently as

$$v_i(\theta, \varphi) = h_i(\theta, \varphi) + \epsilon_i(\theta, \varphi), \quad (11.1)$$

where  $h_i$  is the unknown smooth coordinate function and  $\epsilon_i$  is a zero mean random field, possibly Gaussian. We model cortical thickness  $f$  similarly as

$$f(\theta, \varphi) = g(\theta, \varphi) + e(\theta, \varphi),$$

**FIGURE 11.1**

Parameterization of cortical surface using the spherical coordinates; the north and south poles are chosen in the plane, i.e.  $u_2 = 0$ , that separates the left and the right hemispheres.

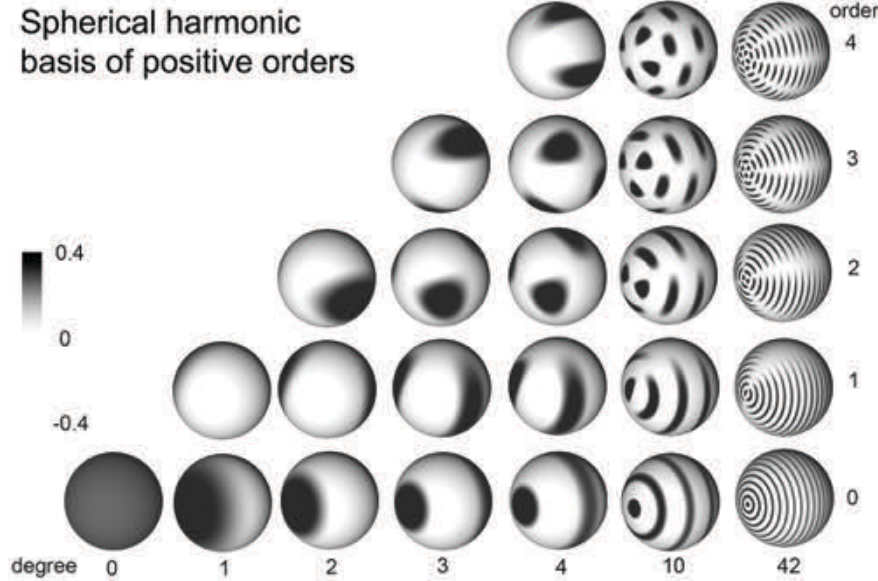
where  $g$  is the unknown mean cortical thickness and  $e$  is a zero mean random field. We further assume  $v_i, f \in \mathcal{L}^2(S^2)$ , the space of square integrable functions on unit sphere  $S^2$ . The unknown signals  $h_i$  and  $g$  are then estimated in the finite subspace of  $\mathcal{L}^2(S^2)$  spanned by harmonic basis functions in least squares fashion.

---

### 11.3 Spherical Harmonics

**Definition 15** *The spherical harmonic  $Y_{lm}$  of degree  $l$  and order  $m$  is defined as*

$$Y_{lm} = \begin{cases} c_{lm} P_l^{|m|}(\cos \theta) \sin(|m|\varphi), & -l \leq m \leq -1, \\ \frac{c_{lm}}{\sqrt{2}} P_l^{|m|}(\cos \theta), & m = 0, \\ c_{lm} P_l^{|m|}(\cos \theta) \cos(|m|\varphi), & 1 \leq m \leq l, \end{cases}$$

**FIGURE 11.2**

Spherical harmonics of positive orders. The negative orders are simply the rotation of the positive order harmonics.

where  $c_{lm} = \sqrt{\frac{2l+1}{2\pi}} \frac{(l-|m|)!}{(l+|m|)!}$  and  $P_l^m$  is the associated Legendre polynomial of order  $m$  [92, 372].

The associated Legendre polynomial is given by

$$P_l^m(x) = \frac{(1-x^2)^{m/2}}{2^l l!} \frac{d^{l+m}}{dx^{l+m}} (x^2 - 1)^l, x \in [-1, 1].$$

The first few terms of the spherical harmonics are

$$\begin{aligned} Y_{00} &= \frac{1}{\sqrt{4\pi}}, Y_{1,-1} = \sqrt{\frac{3}{4\pi}} \sin \theta \sin \varphi, \\ Y_{1,0} &= \sqrt{\frac{3}{4\pi}} \cos \theta, Y_{1,1} = \sqrt{\frac{3}{4\pi}} \sin \theta \cos \varphi. \end{aligned}$$

Few representative spherical harmonics are shown in Figure 11.2. The spherical harmonics are orthonormal with respect to the inner product

$$\langle f_1, f_2 \rangle = \int_{S^2} f_1(\Omega) f_2(\Omega) d\mu(\Omega),$$

where  $\Omega = (\theta, \varphi)$  and the Lebesgue measure  $d\mu(\Omega) = \sin \theta d\theta d\varphi$ . The norm is then defined as

$$\|f_1\| = \langle f_1, f_1 \rangle^{1/2}. \quad (11.2)$$

Consider the subspace  $\mathcal{I}_l$  spanned by the  $l$ -th degree spherical harmonics:

$$\mathcal{I}_l = \left\{ \sum_{m=-l}^l \beta_{lm} Y_{lm}(\Omega) : \beta_{lm} \in \mathbb{R} \right\}.$$

Then the subspace  $\mathcal{H}_k$  spanned by up to  $k$ -th degree spherical harmonics is decomposed as the direct sum of  $\mathcal{I}_0, \dots, \mathcal{I}_k$ :

$$\begin{aligned} \mathcal{H}_k &= \mathcal{I}_0 \oplus \mathcal{I}_1 \cdots \oplus \mathcal{I}_k. \\ &= \left\{ \sum_{l=0}^k \sum_{m=-l}^l \beta_{lm} Y_{lm}(\Omega) : \beta_{lm} \in \mathbb{R} \right\}. \end{aligned}$$

Traditionally, the coordinate functions  $h_i$  are estimated by minimizing the integral of the squared residual within  $\mathcal{H}_k$ :

$$\hat{h}_i(\Omega) = \arg \min_{h \in \mathcal{H}_k} \int_{S^2} |v_i(\Omega) - h(\Omega)|^2 d\mu(\Omega). \quad (11.3)$$

It can be shown that the minimization is obtained when

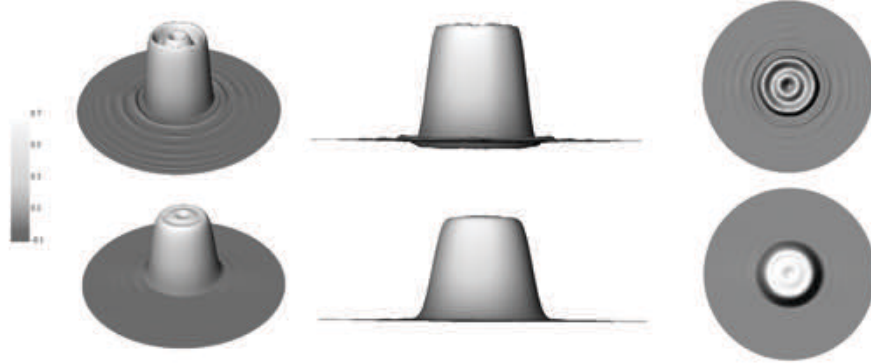
$$\hat{h}_i(\Omega) = \sum_{l=0}^k \sum_{m=-l}^l \langle v_i, Y_{lm} \rangle Y_{lm}(\Omega). \quad (11.4)$$

Representing an anatomical boundary via the Fourier series expansion (11.4) has been referred to as the *spherical harmonic representation* [135, 152, 323, 322]. This technique has been used in representing hippocampi [323], ventricles [135] and cortical surfaces [71, 152].

### 11.3.1 Weighted Spherical Harmonic Representation

The weakness of the traditional spherical harmonic representation is that it produces the Gibbs phenomenon (ringing artifacts) [71, 132] for discontinuous and rapidly changing continuous measurements. The Gibbs phenomenon can be effectively removed if the spherical harmonic representation converges fast enough as the degree goes to infinity. By weighting the spherical harmonic coefficients exponentially smaller, we can make the representation converge faster; this can be achieved by additionally weighting the squared residuals in equation (11.3) with the *heat kernel*.

**Example 8** *Figure 11.3 demonstrates the severe Gibbs phenomenon in the traditional spherical harmonic representation (top row) on a hat-shaped 2D surface. The hat shaped step function is simulated as  $z = 1$  for  $x^2 + y^2 < 1$  and  $z = 0$  for  $1 \leq x^2 + y^2 \leq 2$ . On the other hand the weighted spherical harmonic representation shows substantially reduced ringing artifacts. In both representations, we have used degree  $k = 42$ . For the weighted spherical harmonic representation, the bandwidth  $\sigma = 0.001$  is used throughout the book.*

**FIGURE 11.3**

The Gibbs phenomenon on a hat shaped simulated surface showing the severe ringing effect on the traditional spherical harmonic representation (top) and reduced ringing effect on the weighted spherical harmonic representation (bottom). The degree  $k = 42$  is used for the both cases and the bandwidth  $\sigma = 0.001$  is used for the weighted spherical harmonic representation.

Due to very complex folding patterns, sulcal regions of the brain exhibit more abrupt directional change than the simulated hat surface (upward of 180 degree compared to 90 degree in the hat surface) so there is a need for reducing the Gibbs phenomenon in the traditional spherical harmonic representation.

The heat kernel is the generalization of the Gaussian kernel defined on Euclidean space to an arbitrary Riemannian manifold [76, 304]. On a unit sphere, the heat kernel is written as

$$K_\sigma(\Omega, \Omega') = \sum_{l=0}^{\infty} \sum_{m=-l}^l e^{-l(l+1)\sigma} Y_{lm}(\Omega) Y_{lm}(\Omega'), \quad (11.5)$$

where  $\Omega = (\theta, \varphi)$  and  $\Omega' = (\theta', \varphi')$ . The heat kernel is symmetric and positive definite, and a probability distribution since

$$\int_{S^2} K_\sigma(\Omega, \Omega') d\mu(\Omega) = 1.$$

The parameter  $\sigma$  controls the dispersion of the kernel so we simply call it the *bandwidth*. The heat kernel satisfies

$$\lim_{\sigma \rightarrow \infty} K_\sigma(\Omega, \Omega') = \frac{1}{4\pi} \text{ and } \lim_{\sigma \rightarrow 0} K_\sigma(\Omega, \Omega') = \delta(\Omega - \Omega')$$

with  $\delta$  as the Dirac-delta function. The heat kernel can be further simplified using the harmonic addition theorem [372] as

$$K_\sigma(\Omega, \Omega') = \sum_{l=0}^{\infty} \frac{2l+1}{4\pi} e^{-l(l+1)\sigma} P_l^0(\Omega \cdot \Omega'), \quad (11.6)$$

where  $\cdot$  is the Cartesian inner product.

Let us define *heat kernel smoothing* [76] as

$$K_\sigma * f(\Omega) = \int_{S^2} K(\Omega, \Omega') f(\Omega') d\mu(\Omega'). \quad (11.7)$$

Then heat kernel smoothing has the following spectral representation, which can be easily seen by substituting (11.5) into equation (11.7) and rearranging the integral with the summation:

$$K_\sigma * f(\Omega) = \sum_{l=0}^{\infty} \sum_{m=-l}^l e^{-l(l+1)\sigma} \langle f, Y_{lm} \rangle Y_{lm}(\Omega), \quad (11.8)$$

The  $k$ -th degree finite series approximation of heat kernel smoothing is referred to as the  *$k$ -th degree weighted spherical harmonic representation*. The unknown mean coordinates  $h_i$  are estimated using the weighted spherical harmonic representation, which is the minimizer of the weighted squared distance between measurements  $v_i$  and a function  $h$  in  $\mathcal{H}_k$  space. The unknown mean cortical thickness  $g$  is estimated similarly.

### Theorem 7

$$\begin{aligned} & \sum_{l=0}^k \sum_{m=-l}^l e^{-l(l+1)\sigma} \langle v_i, Y_{lm} \rangle Y_{lm} \\ &= \arg \min_{h \in \mathcal{H}_k} \int_{S^2} \int_{S^2} K_\sigma(\Omega, \Omega') |v_i(\Omega') - h(\Omega)|^2 d\mu(\Omega') d\mu(\Omega) \end{aligned}$$

Theorem 7 is proved as follows. Let  $v_i = \sum_{l=0}^k \sum_{m=-l}^l \beta_{lm} Y_{lm}$ . Let the inner integral be

$$I = \int_{\mathcal{M}} K_\sigma(\Omega, \Omega') \left| v_i(\Omega') - \sum_{l=0}^k \sum_{m=-l}^l \beta_{lm} Y_{lm}(\Omega) \right|^2 d\mu(\Omega').$$

Simplifying the expression, we obtain

$$\begin{aligned} I &= \sum_{l=0}^k \sum_{m=-l}^l \sum_{l'=0}^k \sum_{m'=-l'}^{l'} Y_{lm}(\Omega) Y_{l'm'}(\Omega) \beta_{lm} \beta_{l'm'} \\ &\quad - 2K_\sigma * v_i(\Omega) \sum_{l=0}^k \sum_{m=-l}^l Y_{lm}(\Omega) \beta_{lm} + K * v_i^2(\Omega). \end{aligned}$$

Since  $I$  is an unconstrained positive semidefinite quadratic program (QP) in  $\beta_{lm}$ , there is no unique global minimizer of  $I$  without additional linear constraints. Integrating  $I$  further with respect to  $\mu(\Omega)$ , we collapses the QP to a positive definite QP, which yields a unique global minimizer as

$$\int_{S^2} I d\mu(\Omega) = \sum_{l=0}^k \sum_{m=-l}^l \beta_{lm}^2 - 2 \sum_{i=0}^k e^{-l(l+1)\sigma} \langle v_i, Y_{lm} \rangle \beta_{lm} + \sum_{i=0}^{\infty} e^{-l(l+1)\sigma} \langle v_i^2, Y_{lm} \rangle.$$

The minimum of the above integral is obtained when all the partial derivatives with respect to  $\beta_j$  vanish.

$$\int_{S^2} \frac{\partial I}{\partial \beta_{lm}} d\mu(\Omega) = 2\beta_{lm} - 2e^{-l(l+1)\sigma} \langle v_i, Y_{lm} \rangle = 0.$$

Hence  $\sum_{l=0}^k \sum_{m=-l}^l e^{-l(l+1)\sigma} \langle v_i, Y_{lm} \rangle Y_{lm}$  is the unique minimizer in  $\mathcal{H}_k$ .

We can also show that the weighted spherical harmonic representation is related to previously available surface-based isotropic diffusion smoothing [10, 53, 83, 76] via the following theorem.

### Theorem 8

$$\sum_{l=0}^k \sum_{m=-l}^l e^{-l(l+1)\sigma} \langle v_i, Y_{lm} \rangle Y_{lm}(\Omega) = \arg \min_{h \in \mathcal{H}_k} \|h - h_0\|,$$

where  $h_0$  satisfies isotropic heat diffusion

$$\frac{\partial h_0}{\partial \sigma} = \Delta h_0 = \frac{1}{\sin \theta} \frac{\partial}{\partial \theta} \left( \sin \theta \frac{\partial h_0}{\partial \theta} \right) + \frac{1}{\sin^2 \theta} \frac{\partial^2 h_0}{\partial^2 \varphi}, \quad (11.9)$$

with the initial value condition  $h_0(\Omega, \sigma = 0) = v_i(\Omega)$ .

We first prove that heat kernel smoothing (11.7) and its spectral representation (11.8) are the solution of the heat equation (11.9). At each fixed  $\sigma$ , which serves as the physical time of the heat equation, the solution  $h_0(\Omega, \sigma)$  belongs to  $\mathcal{L}^2(S^2)$ . Then the solution can be written as

$$h_0(\Omega, \sigma) = \sum_{l=0}^{\infty} \sum_{m=-l}^l c_{lm}(\sigma) Y_{lm}(\Omega). \quad (11.10)$$

Since the spherical harmonics are the eigenfunctions of the spherical Laplacian [372], we have

$$\Delta Y_{lm}(\Omega) = -l(l+1)Y_{lm}(\Omega). \quad (11.11)$$

Substituting (11.10) into (11.9) and using (11.11), we obtain

$$\frac{\partial c_{lm}(\sigma)}{\partial \sigma} = -l(l+1)c_{lm}(\sigma). \quad (11.12)$$

The solution of the ordinary differential equation (11.12) is given by  $c_{lm}(\sigma) = b_{lm}e^{-l(l+1)\sigma}$  for some constant  $b_{lm}$ . Hence, we obtain the solution of the form

$$h_0(\Omega, \sigma) = \sum_{l=0}^{\infty} \sum_{m=-l}^l b_{lm} e^{-l(l+1)\sigma} Y_{lm}(\Omega).$$

When  $\sigma = 0$ , we have the initial condition

$$h_0(\Omega, 0) = \sum_{l=0}^{\infty} \sum_{m=-l}^l b_{lm} Y_{lm}(\Omega) = v_i(\Omega).$$

The coefficients  $b_{lm}$  must be the spherical harmonic coefficients, i.e.  $b_{lm} = \langle v_i, Y_{lm} \rangle$ . Then from the property of the generalized Fourier series [307], the finite expansion is the closest to the infinite series in  $\mathcal{H}_k$ :

$$\sum_{l=0}^k \sum_{m=-l}^l e^{-l(l+1)\sigma} \langle v_i, Y_{lm} \rangle Y_{lm}(\Omega) = \arg \min_{h \in \mathcal{H}_k} \|h - h_0(\Omega, \sigma)\|.$$

This proves the statement of the theorem.

### 11.3.2 Estimating Spherical Harmonic Coefficients

The spherical harmonic coefficients are estimated based on an iterative procedure that utilizes the orthonormality of spherical harmonics. We assume that coordinate functions are measured at  $n$  points  $\Omega_1, \dots, \Omega_n$ . Then we have the normal equations

$$v_i(\Omega_j) = \sum_{l=0}^k \sum_{m=-l}^l e^{-l(l+1)\sigma} \langle v_i, Y_{lm} \rangle Y_{lm}(\Omega_j), j = 1, \dots, n. \quad (11.13)$$

The normal equations (11.13) can be written in the matrix form as

$$\mathbf{V} = \underbrace{[\mathbf{Y}_0, e^{-1(1+1)\sigma} \mathbf{Y}_1, \dots, e^{-k(k+1)\sigma} \mathbf{Y}_k]}_{\mathbf{Y}} \beta, \quad (11.14)$$

where the column vectors are

$$\begin{aligned} \mathbf{V} &= [v_i(\Omega_1), \dots, v_i(\Omega_n)]' \\ \beta' &= (\beta'_0, \beta'_1, \dots, \beta'_k) \end{aligned}$$

with  $\beta'_l = (\langle v_i, Y_{l,-l} \rangle, \dots, \langle v_i, Y_{l,l} \rangle)$ . The length of the vector  $\beta$  is

$$1 + (2 \cdot 1 + 1) + \dots + (2 \cdot k + 1) = (k + 1)^2.$$

Each submatrix  $\mathbf{Y}_l$  is given by

$$\mathbf{Y}_l = \begin{bmatrix} Y_{l,-l}(\Omega_1), & \dots, & Y_{l,l}(\Omega_1) \\ \vdots & \ddots & \vdots \\ Y_{l,-l}(\Omega_n), & \dots, & Y_{l,l}(\Omega_n) \end{bmatrix}.$$

We may tempted to directly estimate  $\beta$  in least squares fashion as

$$\hat{\beta} = (\mathbf{Y}'\mathbf{Y})^{-1}\mathbf{Y}'\mathbf{V}.$$

However, since the size of matrix  $\mathbf{Y}'\mathbf{Y}$  becomes  $(k+1)^2 \times (k+1)^2$ , for large degree  $k$ , it may be difficult to directly invert the matrix. Instead of directly solving the normal equations, we project the normal equations into a smaller subspace  $\mathcal{I}_l$  and estimate  $2l+1$  coefficients in an iterative fashion.

At degree 0, we write  $\mathbf{V} = \mathbf{Y}_0\beta_0 + \mathbf{r}_0$ , where  $\mathbf{r}_0$  is the residual vector of estimating  $\mathbf{V}$  in subspace  $\mathcal{I}_0$ . Note that the residual vector  $\mathbf{r}_0$  consists of residuals  $r_0(\Omega_j)$  for all  $\Omega_j$ . Then we estimate  $\beta_0$  by minimizing the residual vector in least squares fashion:

$$\hat{\beta}_0 = (\mathbf{Y}'_0\mathbf{Y}_0)^{-1}\mathbf{Y}'_0\mathbf{V} = \frac{\sum_{j=1}^n v_i(\Omega_j)Y_{00}(\Omega_j)}{\sum_{j=1}^n Y_{00}^2(\Omega_j)}.$$

At degree  $l$ , we have

$$\mathbf{r}_{l-1} = e^{-l(l+1)\sigma}\mathbf{Y}_l\beta_l + \mathbf{r}_l, \quad (11.15)$$

where the residual vector  $\mathbf{r}_{l-1}$  is obtained from the previous estimation as

$$\mathbf{r}_{l-1} = \mathbf{V} - \mathbf{Y}_0\hat{\beta}_0 - \dots - e^{-(l-1)l\sigma}\mathbf{Y}_{l-1}\hat{\beta}_{l-1}.$$

The least squares minimization of  $\mathbf{r}_l$  is then given by

$$\hat{\beta}_l = e^{l(l+1)\sigma}(\mathbf{Y}'_l\mathbf{Y}_l)^{-1}\mathbf{Y}'_l\mathbf{r}_{l-1}.$$

The correctness of the algorithm can be easily seen from

$$\begin{aligned} & \sum_{m=-l}^l e^{-l(l+1)\sigma} \langle v_i, Y_{lm} \rangle Y_{lm} \\ &= \arg \min_{h \in \mathcal{I}_l} \int_{S^2} K_\sigma(\Omega, \Omega') \left| r_{l-1}(\Omega') - h(\Omega) \right|^2 d\mu(\Omega'), \end{aligned}$$

where the residual is given by

$$r_l(\Omega') = v_i(\Omega') - \sum_{l'=0}^l \sum_{m=-l'}^{l'} e^{-l(l+1)\sigma} \langle v_i, Y_{lm} \rangle Y_{lm}(\Omega').$$

This iterative algorithm is referred to as the *iterative residual fitting (IRF)* algorithm [71] since we are iteratively fitting a linear equation to the residuals obtained from the previous iteration. The IRF algorithm is similar to the *matching pursuit method* [240] although the IRF was developed independently. The IRF algorithm was developed to avoid the computational burden of inverting a huge linear problem while the matching pursuit method was

originally developed to compactly decompose a time frequency signal into a linear combination of a pre-selected pool of basis functions.

In the IRF algorithm, we minimize the residual component  $\mathbf{r}_l$  in least squares fashion, i.e. minimizing the sum of squared residuals  $\sum_{j=1}^n r_l^2(\Omega_j)$  over all mesh vertices. On the other hand, in the marching pursuit method, the norm  $\|\mathbf{Y}_l \beta_l\|^2$  is maximized. Due to orthonormality, maximizing the norm is equivalent to minimizing the norm of the residual

$$\|\mathbf{r}_l\|^2 = \int_{S^2} r_l^2(\Omega) d\mu(\Omega).$$

So there is a slight difference in how the residual is minimized. Although there is no limitation estimating multiple coefficients simultaneously in the matching pursuit method, [240] only deals with the problem of estimating one coefficient at a time rather than multiple coefficients as in the IRF algorithm.

Although increasing the degree of the representation increases the goodness-of-fit, it also increases the number of estimated coefficients quadratically. So it is necessary to stop the iteration at the specific degree  $k$ , where the goodness-of-fit and the number of coefficients balance out. From (11.1), we can see that the  $k$ -th degree weighted spherical harmonic representation can be modeled as a linear model setting:

$$v_i(\Omega_j) = \sum_{l=0}^k \sum_{m=-l}^l e^{-l(l+1)\sigma} \beta_{lm}^i Y_{lm}(\Omega_j) + \epsilon_i(\Omega_j),$$

where the least squares estimation of  $\beta_{lm}^i$  is  $\widehat{\beta}_{lm}^i = \langle v_i, Y_{lm} \rangle$ . Then we stop the iteration at degree  $k$  by testing if the  $2k+3$  coefficients at the next iteration vanish:

$$H_0 : \beta_{k+1,-(k+1)}^i = \beta_{k+1,-k}^i = \cdots = \beta_{k+1,k+1}^i = 0.$$

If we assume  $\epsilon_i$  to be a Gaussian random field, the usual  $F$  test at the significant level  $\alpha = 0.01$  can be used to determine the stopping degree. In our study, at bandwidth  $\sigma = 0.001$ , we stop the iteration at degree  $k = 42$ .

### 11.3.3 Validation Against Heat Kernel Smoothing

The weighted spherical harmonic representation is validated against heat kernel smoothing as formulated in [76]. Heat kernel smoothing was implemented as an iterated weighted averaging technique, where the weights are spatially adapted to follow the shape of heat kernel in discrete fashion along a surface mesh. The algorithm has been implemented in MATLAB and it is freely available at [www.stat.wisc.edu/~mchung/softwares/hk/hk.html](http://www.stat.wisc.edu/~mchung/softwares/hk/hk.html). Since its introduction in 2005, the method has been used in smoothing various cortical surface data: cortical curvatures [235, 130], cortical thickness [234, 38], hippocampus [324, 411], magnetoencephalography (MEG) [161] and functional-MRI [157, 186].

**Definition 16** The  $n$ -th iterated heat kernel smoothing of signal  $f \in L^2(S^2)$  is

$$K_\sigma^{(n)} * f(\Omega) = \underbrace{K_\sigma * \cdots * K_\sigma}_{n \text{ times}} * f(\Omega).$$

Then we have the following theorem.

**Theorem 9 3**  $K_\sigma * f(\Omega) = K_{\sigma/n}^{(n)} * f(\Omega)$ .

By letting  $f = Y_{l'm'}$  in (11.8), and using the orthonormality of spherical harmonics, we obtain

$$K_\sigma * Y_{l'm'}(\Omega) = \int_{S^2} K_\sigma(\Omega, \Omega') Y_{l'm'}(\Omega') d\mu(\Omega') = e^{-(l'+1)l'\sigma} Y_{l'm'}(\Omega).$$

This is the restatement of the fact that  $e^{-l(l+1)}\sigma$  and  $Y_{l'm'}$  are eigenvalues and eigenfunctions of the above integral equation with heat kernel. By reapplying heat kernel smoothing to (11.8), we obtain

$$K_\sigma^{(2)} * f(\Omega) = \sum_{l=0}^{\infty} \sum_{m=-l}^l e^{-l(l+1)\sigma} \langle f, Y_{lm} \rangle K_\sigma * Y_{lm}(\Omega) \quad (11.16)$$

$$= \sum_{l=0}^{\infty} \sum_{m=-l}^l e^{-l(l+1)2\sigma} \langle f, Y_{lm} \rangle Y_{lm}(\Omega). \quad (11.17)$$

Then, arguing inductively, we obtain the spectral representation of the  $n$ -th iterated heat kernel smoothing as

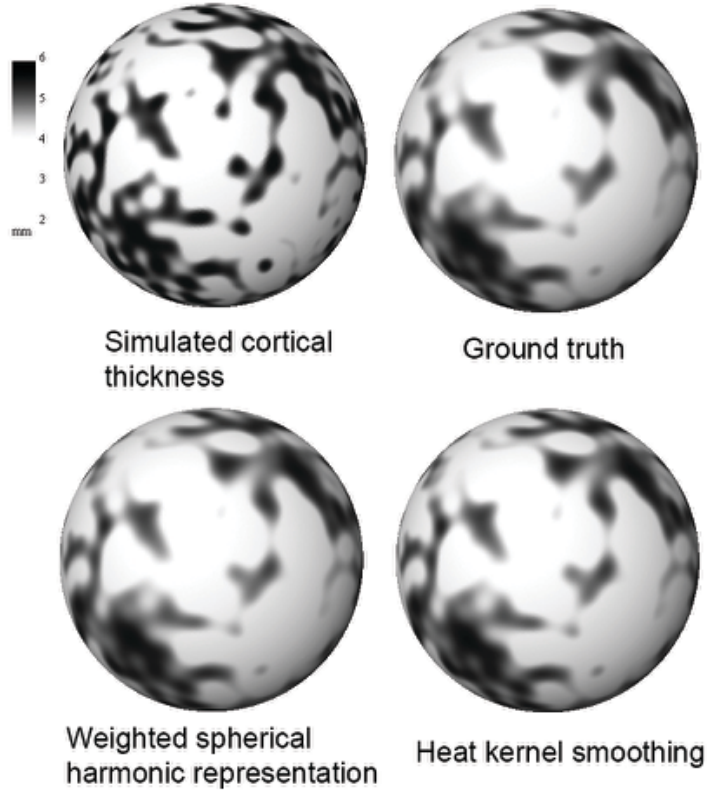
$$K_\sigma^{(n)} * f(\Omega) = \sum_{l=0}^{\infty} \sum_{m=-l}^l e^{-l(l+1)n\sigma} \langle f, Y_{lm} \rangle Y_{lm}(\Omega).$$

The right side is the spectral representation of heat kernel smoothing with bandwidth  $n\sigma$ . This proves  $K_\sigma^{(n)} * f(\Omega) = K_{n\sigma} * f(\Omega)$ . Rescaling the bandwidth, we obtain the result.

Theorem 3 shows that heat kernel smoothing with large bandwidth  $\sigma$  can be decomposed into  $n$  repeated applications of heat kernel smoothing with smaller bandwidth  $\sigma/n$ . When the bandwidth is small, the heat kernel behaves like the Dirac-delta function and, using the *parametrix expansion* [304, 374], we can approximate it locally using the Gaussian kernel:

$$K_\sigma(\Omega, \Omega') = \frac{1}{\sqrt{4\pi}\sigma} \exp \left[ -\frac{d^2(\Omega, \Omega')}{4\sigma} \right] [1 + O(\sigma^2)], \quad (11.18)$$

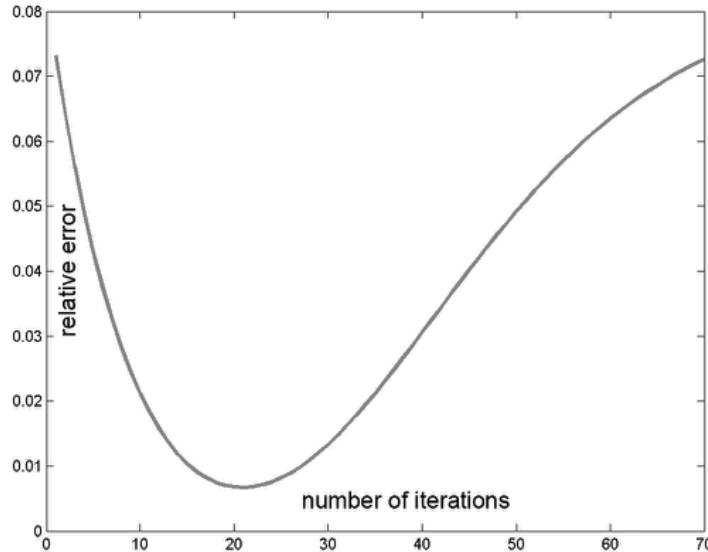
where  $d(p, q)$  is the geodesic distance between  $p$  and  $q$ . For small bandwidth, all the kernel weights are concentrated near the center, so we need only to worry about the first neighbors of a given vertex in a surface mesh.

**FIGURE 11.4**

Cortical thickness is simulated from the sample cortical thickness. The ground truth is analytically constructed from the simulation. Then the weighted spherical harmonic representation and heat kernel smoothing of the simulated cortical thickness are compared against the ground truth for validation.

Let  $\Omega_1, \dots, \Omega_m$  be  $m$  neighboring vertices of vertex  $\Omega = \Omega_0$  in the mesh. The geodesic distance between  $\Omega$  and its adjacent vertex  $\Omega_i$  is the length of edge between these two vertices in the mesh. Then the discretized and normalized heat kernel is given by

$$W_\sigma(\Omega, \Omega_i) = \frac{\exp\left(-\frac{d(\Omega, \Omega_i)^2}{4\sigma}\right)}{\sum_{j=0}^m \exp\left(-\frac{d(\Omega, \Omega_j)^2}{4\sigma}\right)}.$$

**FIGURE 11.5**

The plot is the relative error over the number of iterations for heat kernel smoothing against the ground truth.

Note that  $\sum_{i=0}^m W_\sigma(\Omega, \Omega_i) = 1$ . The discrete version of heat kernel smoothing on a triangle mesh is then defined as

$$W_\sigma * f(\Omega) = \sum_{i=0}^m W_\sigma(\Omega, \Omega_i) f(\Omega_i).$$

The discrete kernel smoothing should converge to heat kernel smoothing (11.7) as the mesh resolution increases. This is the form of the *Nadaraya-Watson estimator* [63] applied to surface data. Instead of performing a single kernel smoothing with large bandwidth  $n\sigma$ , we perform  $n$  iterated kernel smoothing with small bandwidth  $\sigma$  as follows  $W_\sigma^{(n)} * f(\Omega)$ .

For comparison between the weighted spherical harmonic representation and heat kernel smoothing, we used the sample cortical thickness data in constructing the analytical ground truth. Consider a surface measurement of the form

$$f(\Omega) = \sum_{l=0}^k \sum_{m=-l}^l \beta_{lm} Y_{lm}(\Omega) \quad (11.19)$$

for some given  $\beta_{lm}$ . Heat kernel smoothing of  $f$  is given as an exact analytic form, which serves as the ground truth for validation:

$$K_\sigma * f(\Omega) = \sum_{l=0}^k \sum_{m=-l}^l e^{-l(l+1)\sigma} \beta_{lm} Y_{lm}(\Omega). \quad (11.20)$$

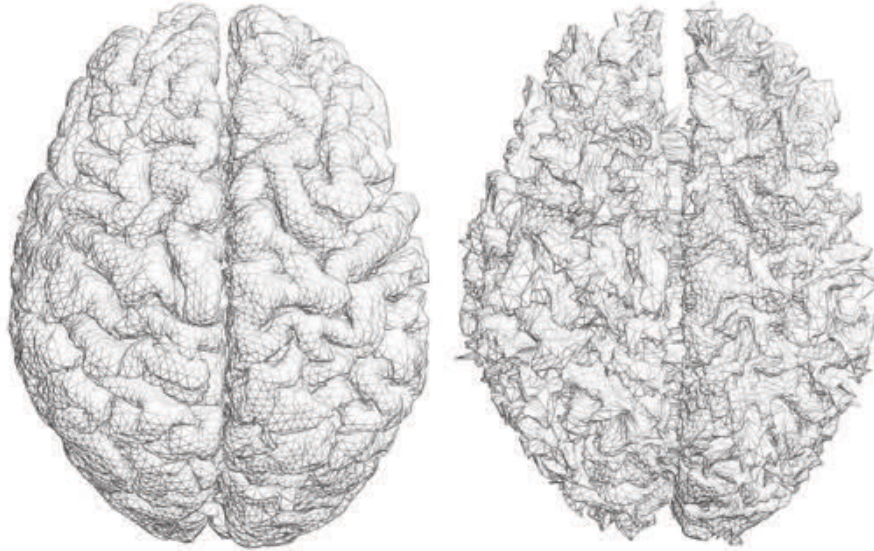
Using the sample cortical thickness data, we simulated the measurement of the form (11.19) by estimating  $\beta_{lm} = \langle f, Y_{lm} \rangle$  (Figure 11.4 top left). Then we compared the weighted spherical harmonic representation of  $f$  and the discrete version of heat kernel smoothing  $W_{\sigma/n}^{(n)} * f$  against the analytical ground truth (11.20) (Figure 11.4 top right) along the surface mesh.

For the weighted spherical harmonic representation, we used  $\sigma = 0.001$  and the corresponding optimal degree  $k = 42$  (Figure 11.4 bottom left). The relative error for the weighted spherical harmonic representation is up to 0.013 at a certain vertex and the mean relative error over all mesh vertices is 0.0012. For heat kernel smoothing, we used varying numbers of iterations,  $1 \leq n \leq 70$ , and the corresponding bandwidth  $\sigma = 0.001/n$ . The performance of heat kernel smoothing depended on the number of iterations, as shown in the plot of relative error over the number of iterations in Figure 11.5. The minimum relative error was obtained when 21 iterations were used. The relative error was up to 0.055 and the mean relative error was 0.0067. Our simulation result demonstrates that the weighted spherical harmonic representation performs better than heat kernel smoothing. The main problem with heat kernel smoothing is that the number of iterations needs to be predetermined, possibly using the proposed simulation technique. Even at the optimal iteration of 21, the weighted spherical harmonic representation provides a better performance.

## 11.4 Weighted-SPHARM Package

The cortical surface data we will use here as an example was first published in [76]. 16 high functioning autistic and 11 normal control subjects used in this study were screened to be right-handed males. There are 12 control subjects in [76]; however, one subject is removed due to image processing artifacts.

Age distributions for HFA and NC are  $15.93 \pm 4.71$  and  $17.08 \pm 2.78$  respectively. High resolution anatomical magnetic resonance images (MRI) were obtained using a 3-Tesla GE SIGNA (General Electric Medical Systems, Waukesha, WI) scanner with a quadrature head RF coil. A three-dimensional, spoiled gradient-echo (SPGR) pulse sequence was used to generate  $T_1$ -weighted images. The imaging parameters were TR/TE = 21/8 ms, flip angle =  $30^\circ$ , 240 mm field of view, 256x192 in-plane acquisition matrix (interpolated on the scanner to 256x256), and 128 axial slices (1.2 mm thick) covering the whole brain.

**FIGURE 11.6**

Outer and inner cortical surface meshes of a subject. Each surface consists of 40962 vertices and 81920 triangles. Vertices across subjects match anatomically so there is no need for the additional surface alignment.

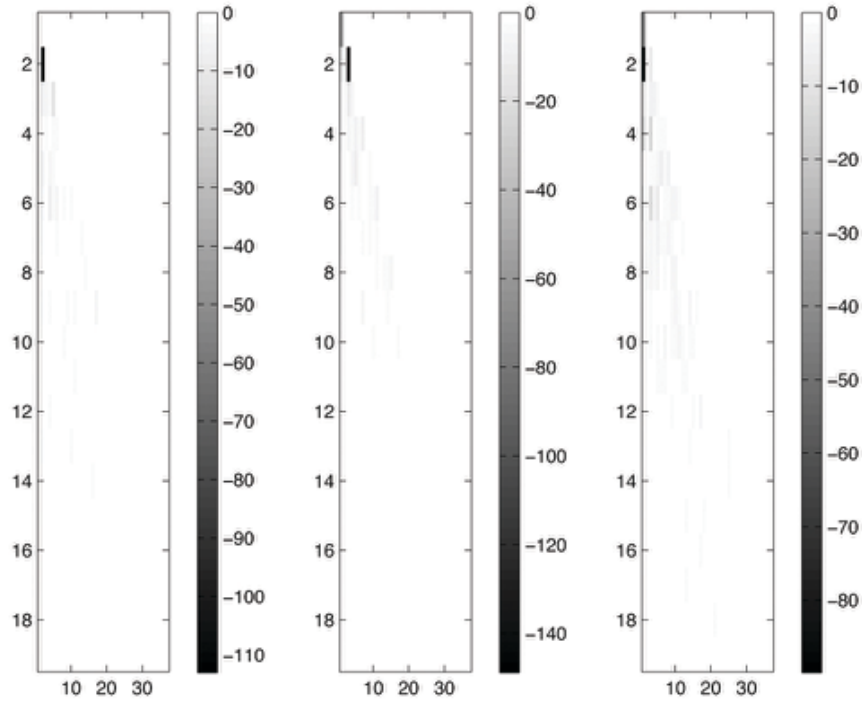
Following image processing steps described in [76], both the outer and inner cortical surfaces were extracted for each subject via a deformable surface algorithm [237]. Surface normalization is performed by minimizing an objective function that measures the global fit of two surfaces while maximizing the smoothness of the deformation in such a way that the pattern of gyral ridges is matched smoothly [301, 76].

The surface data stored in `autism.surface.mat` consists of coordinates of the both inner and outer cortical surfaces of 27 subjects (16 autistic and 11 control) and ages in years. `autisminner` and `autismouter` are matrices of size  $16 \times 3 \times 40962$  while `controlinner` and `controlouter` are matrices of size  $11 \times 3 \times 40962$ .

The MATLAB codes for performing the weighted-SPHARM representation are given in <http://brainimaging.waisman.wisc.edu/~chung/BIA>. The cortical surfaces of the first autistic subjects can be visualized using the commands (Figure 11.6)

```
load autism.surface.mat

surf.vertices=squeeze(autisminner(1,:,:));
surf.faces=tri;
figure; figure_wire(surf, 'yellow', 'white');
```

**FIGURE 11.7**

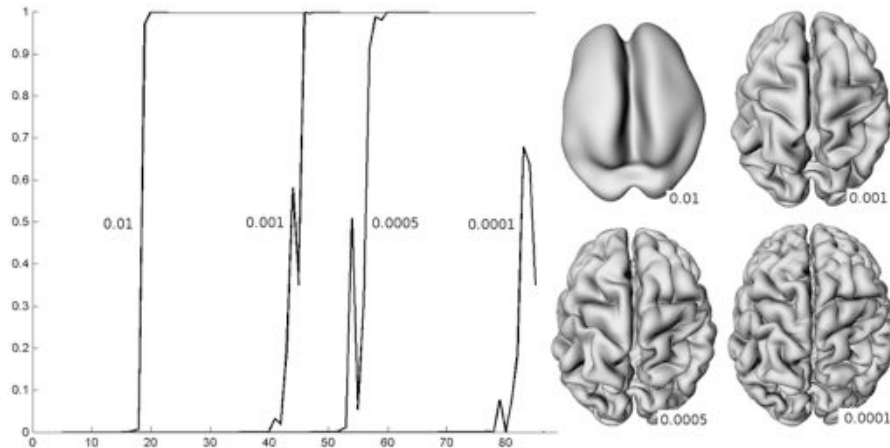
Spherical harmonic coefficients up to degree 18 are stored as a triangle matrix of size  $19 \times 37$ . The vertical axis is degree and the horizontal axis is order. The coefficient of degree  $l$  and order  $m$  is displayed in the position  $(l, m + 19)$ .

```
surf.vertices=squeeze(autismouter(1,:,:))';
surf.faces=tri;
figure; figure_wire(surf, 'yellow', 'white');
```

SPHARM representation requires a unit sphere mesh `sphere40962.mat` that corresponds to the cortical surfaces. Then we establish the spherical angles on the cortical surfaces using

```
load sphere40962.mat
[theta varphi]=SPHARMangles(sphere40962);
figure; figure_trimesh(surf,theta,'rwb');
figure; figure_trimesh(surf,varphi,'rwb');
```

The angles `theta` and `varphi` can be displayed either on the unit sphere or the cortical surface (Figure 11.6). Using the spherical angles, we construct the weighted-SPHARM.

**FIGURE 11.8**

Cortical thickness projected onto the average outer cortex for various  $t$  and corresponding optimal degree:  $k = 18(\sigma = 0.01)$ ,  $k = 42(\sigma = 0.001)$ ,  $k = 52(\sigma = 0.0005)$ ,  $k = 78(\sigma = 0.0001)$ . The average cortex is constructed by averaging the coefficients of the weighted-SPHARM. The highly noise first image shows thickness measurements obtained by computing the distance between two triangle meshes.

```
[surfsmooth, fourier]=SPHARMSmooth2(surf,sphere40962,18,0.01);
figure_wire(surfsmooth,'yellow','white');
```

This constructs the weighted-SPHARM representation of the outer cortical surface with  $k = 18$  and  $\sigma = 0.01$  (Figure 11.8). It requires exactly identical mesh topology between `surf` and `sphere4092`. `surfsmooth` is the smoothed surface of the form

```
surfsmooth =
vertices: [40962x3 double]
faces: [81920x3 double]
```

while `fourier` is a structured array of spherical harmonic coefficients for all  $x$ ,  $y$ , and  $z$ -coordinates. The spherical harmonic coefficients can be extracted possibly for data reduction and classification purposes. For each representation, we have Fourier coefficients for  $x, y$  and  $z$  coordinates.

```
fourier =
x: [19x37 double]
y: [19x37 double]
```

```

z: [19x37 double]

figure;
subplot(1,3,1)
imagesc(-abs(fourier.x)); colorbar
subplot(1,3,2)
imagesc(-abs(fourier.y)); colorbar;
subplot(1,3,3)
imagesc(-abs(fourier.z)); colorbar
colormap('gray'); figure_bg('white')

```

The first dimension in `fourier.x` is the degree between 0 and 18 and the second dimension is the order between -18 and 18. See Figure 11.7 for the display of the Fourier coefficients for subject 1. For the  $l$ -th degree, there are total  $2l+1$  orders so not all elements in the matrix contain Fourier coefficients. Figure 11.7 shows the upper triangle elements are padded with zeros. Since it is difficult to handle the coefficients in a matrix form, we vectorize them using `SPHARMvectorize` command.

```

fourierv = SPHARMvectorize(fourier,18)

fourierv =

```

$$\begin{aligned} \text{x: } &[1 \times 361 \text{ double}] \\ \text{y: } &[1 \times 361 \text{ double}] \\ \text{z: } &[1 \times 361 \text{ double}] \end{aligned}$$

There are total  $1 + (2 + 1) + (2 \times 2 + 1) + \dots + (2 \times 18 + 1) = (18 + 1)^2 = 361$  Fourier coefficients for each coordinate.

Using the estimated coefficients `fourier`, we can reconstruct smoothed cortical surfaces with the different amount of smoothing. Once the coefficients are estimated once, we can reuse them without reestimating them again. Using `SPHARMrepresent2.m`, 18 degree weighted-SPHARM representation with different bandwidth  $\sigma = 0, 0.01, 0.1$  can be obtained (Figure 11.9).

```

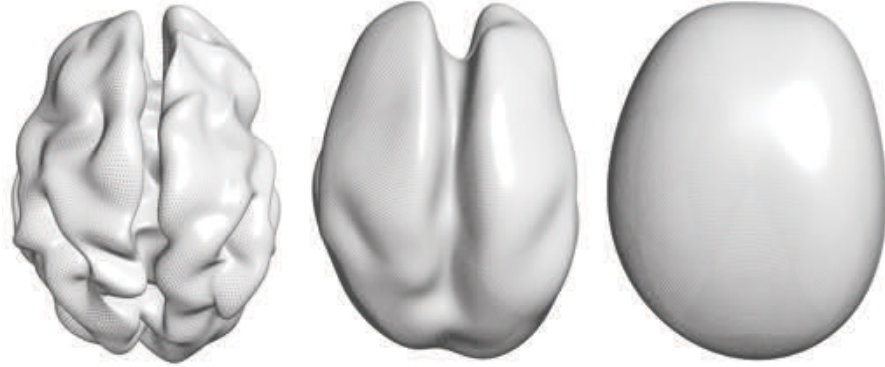
surf=SPHARMrepresent2(sphere40962, fourier, 18,0);
figure; figure_wire(surf,'white','white');

surf=SPHARMrepresent2(sphere40962, fourier, 18,0.01);
figure; figure_wire(surf,'white','white');

surf=SPHARMrepresent2(sphere40962, fourier, 18,0.1);
figure; figure_wire(surf,'white','white');

```

The spherical harmonic representation can be used to establish surface correspondence between different subjects. The concept is introduced in [71].

**FIGURE 11.9**

The weighted spherical harmonic representation with degree 18 and  $\sigma = 0, 0.01, 0.1$ . Even at the same degree, the changes in the bandwidth  $\sigma$  drastically change the shape of brain.

## 11.5 Surface Registration

Previously cortical surface normalization was performed by minimizing an objective function that measures the global fit of two surfaces while maximizing the smoothness of the deformation in such a way that the gyral patterns are matched smoothly [76, 301, 363]. In the spherical harmonic representation, the surface normalization is straightforward and does not require any sort of optimization explicitly but at least requires some initial alignment. A crude alignment can be done by coinciding the first order ellipsoid meridian and equator in the SPHARM-correspondence approach [135, 344]. For cortical meshes obtained using the anatomic segmentation using the proximities (ASP) algorithm [237], such alignments are not needed. An approximate surface alignment is done during the cortical surface extraction process. The algorithm generates 40,962 vertices and 81,920 triangles with the identical mesh topology for all subjects. The vertices indexed identically on two cortical meshes will have a very close anatomic homology and this defines the surface alignment. This provides the same spherical parameterization at identically indexed vertices across different cortical surfaces.

Consider a surface  $h = (h_1, h_2, h_3)$  obtained from the coordinates  $v_i$  measured at point  $p$ :

$$h_i(p) = \sum_{l=0}^k \sum_{m=-l}^l \langle v_i, Y_{lm} \rangle(p).$$

Consider another surface  $j_i$  obtained from coordinate functions  $w_i$ :

$$j_i(p) = \sum_{l=0}^k \sum_{m=-l}^l \langle w_i, Y_{lm} \rangle(p).$$

Suppose the surface  $h_i$  is deformed to  $h_i + d_i$  under the influence of the displacement vector field  $d_i$ . We wish to find  $d_i$  that minimizes the discrepancy between  $h_i + d_i$  and  $j_i$  in the finite subspace  $\mathcal{H}_k$ . This can be easily done by noting that

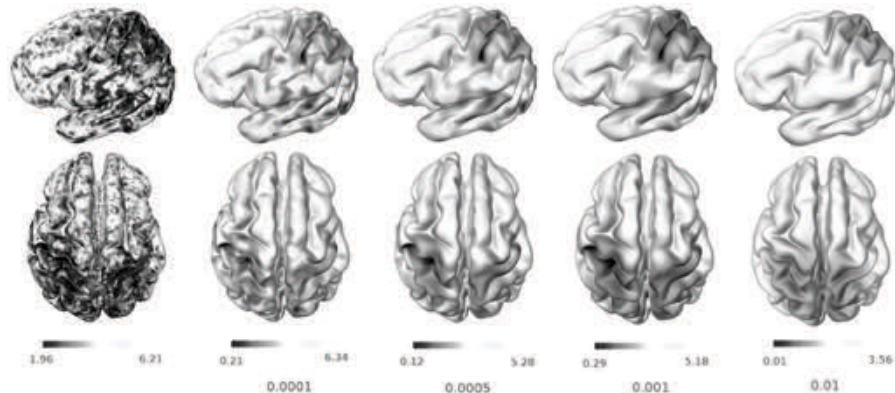
$$\sum_{l=0}^k \sum_{m=-l}^l (w_{lm}^i - v_{lm}^i) Y_{lm}(p) = \arg \min_{d_i \in \mathcal{H}_k} \left\| \hat{h}_i + d_i - \hat{j}_i \right\|. \quad (11.21)$$

This implies that the optimal displacement in the least squares sense is obtained by simply taking the difference between two weighted spherical harmonic representations and matching coefficients of the same degree and order. Then a specific point  $\hat{h}_i(p_0)$  in one surface corresponds to  $\hat{j}_i(p_0)$  in the other surface. We refer to this point-to-point surface correspondence as the *spherical harmonic correspondence* [71]. The spherical harmonic correspondence shows that the optimal displacement in the least squares sense is obtained by simply taking the difference between two spherical harmonic representations. Unlike other surface registration methods used in warping surfaces between subjects [76, 301, 363], it is not necessary to consider an additional cost function that guarantees the smoothness of the displacement field since the displacement field  $d = (d_1, d_2, d_3)$  is already a linear combination of smooth basis functions.

The previously available approaches for computing the cortical thickness in discrete triangle meshes produce noisy thickness measures [76, 120, 237]. So it is necessary to smooth the thickness measurements along the cortex via surface-based smoothing techniques [10, 54, 53, 83]. On the other hand, the weighted-SPHARM provides smooth functional representation of the outer and inner surfaces so that the distance measures between the surfaces should be already smooth. Hence, the weighted-SPHARM avoids the additional step of thickness smoothing done in most of thickness analysis literature [76, 83] while it is not necessary to perform data smoothing in the spherical harmonic formulation. The distance between the outer and inner cortical surfaces can be determined using the spherical harmonic correspondence. Given the outer surface  $h_i$  and the inner surface  $j_i$ , the cortical thickness is defined to be the Euclidean distance between the two representations:

$$\text{thick}(p) = \sqrt{\sum_{i=1}^3 \left[ \sum_{l=0}^k \sum_{m=-l}^l \langle v_i - w_i, Y_{lm} \rangle \right]^2}.$$

A similar approach has been proposed for measuring the closeness between two surfaces [135]. Figure 11.10 shows the comparison of cortical thickness computed from the traditional deformable surface algorithm [237] and the

**FIGURE 11.10**

Cortical thickness of a subject projected onto a template. The cortical thickness is computed from the spherical harmonic correspondence with heat kernel weights. As the bandwidth increases from  $\sigma = 0.0001$  to  $0.01$ , the amount of smoothing also increases. The first image shows the cortical thickness obtained from the traditional deformable surface algorithm [237].

spherical harmonic correspondence. The cortical thickness obtained from the traditional approach introduces a lot of triangle mesh noise into its estimation while the spherical harmonic correspondence approach does not. The spatial smoothness of the thickness is explicitly incorporated via the bandwidth  $\sigma$ .

### 11.5.1 MATLAB implementation

The SPHARM-correspondence will be explained using `autism.surface.mat`. We will first compute the cortical thickness of the autistic subjects 1 and 2.

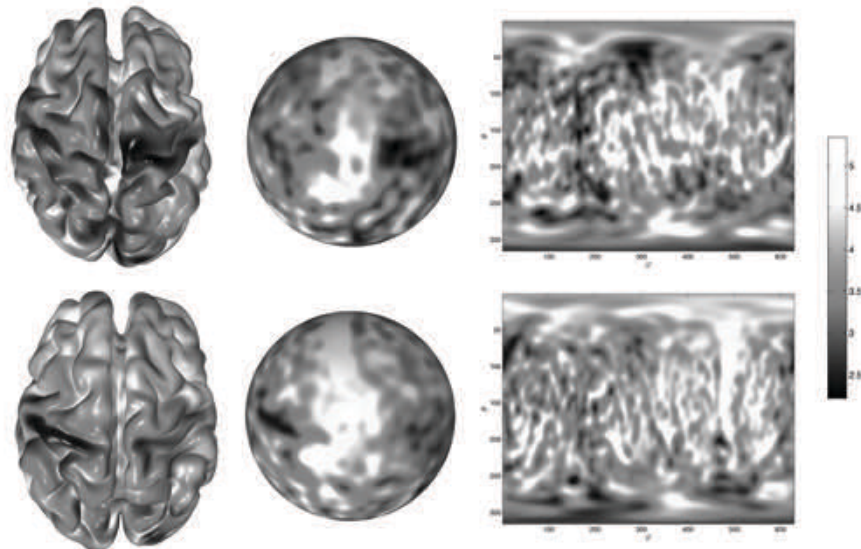
```

load autism.surface.mat
surfout1.vertices=squeeze(autismouter(1,:,:))';
surfout1.faces=tri;
surfin1.vertices=squeeze(autisminner(1,:,:))';
surfin1.faces=tri;

surfout2.vertices=squeeze(autismouter(2,:,:))';
surfout2.faces=tri;
surfin2.vertices=squeeze(autisminner(2,:,:))';
surfin2.faces=tri;

thick1 = L2norm(surfout1.vertices-surfin1.vertices);
thick2 = L2norm(surfout2.vertices-surfin2.vertices);

```

**FIGURE 11.11**

Cortical thickness of subjects 1 and 2. Cortical thickness has been smoothed using weighted-SPHARM with degree 42 and bandwidth  $\sigma = 0.001$ . The cortical surfaces are also smoothed using the same parameters. The cortical thickness maps are also projected onto a unit sphere for better visualization. SPHARM framework can be used to establish the point-wise correspondence between the surfaces.

`thick1` and `thick2` are the cortical thickness of subjects 1 and 2. This is simply computed as the Euclidian distance between the outer and inner cortical surfaces using `L2norm` function. Then we compute the weighted-SPHARM representation of the surfaces and their thickness with degree 42 and bandwidth  $\sigma = 0.001$ .

```

load sphere40962.mat
[surfout1,fourier1]=SPHARMSmooth2(surfout1,sphere40962,42,0.001);
[surfout2,fourier2]=SPHARMSmooth2(surfout2,sphere40962,42,0.001);

surfthick1.vertices=[thick1 thick1 thick1];
surfthick1.faces=tri;
[surfthick1,fourier]=SPHARMSmooth2(surfthick1,sphere40962,42,0.001);
thick1smooth = surfthick1.vertices(:,1);

surfthick2.vertices=[thick2 thick2 thick2];
surfthick2.faces=tri;

```

```
[surfthick2,fourier]=SPHARMsmooth2(surfthick2,sphere40962,42,0.001);
thick2smooth = surfthick2.vertices(:,1);
```

In order to smooth cortical thickness, `thick1` is treated as the coordinate of the mesh vertices in `surfthick1.vertices=[thick1 thick1 thick1]` and feeds into `SPHARMsmooth2` routine. The cortical thickness of subject 1 is visualized as Figure 11.11 using `figure_trimesh`.

```
figure; figure_trimesh(surfout1,thick1smooth);
colormap('hot')
shading interp
view([0 90])
camlight headlight

figure; figure_trimesh(sphere40962, thick1smooth);
colormap('hot')
shading interp
view([0 90])
camlight headlight
```

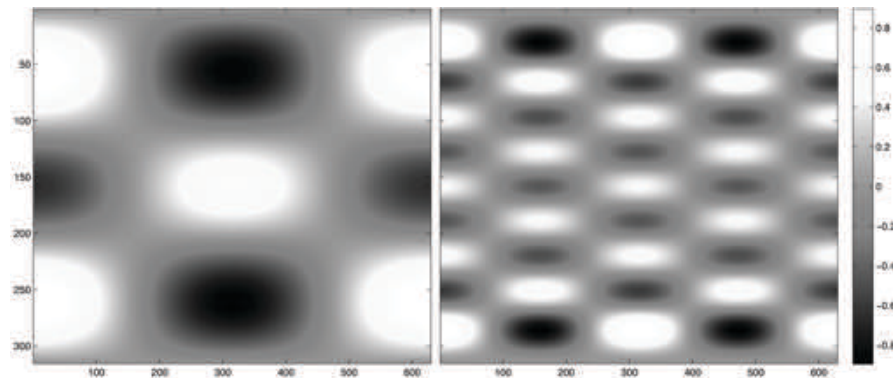
The subject 2 is displayed similarly. Cortical thickness is defined along a curved cortical surface. For flattening the thickness map onto a sphere, we can simply use the spherical mesh `sphere40962` that is topologically equivalent to the cortical mesh. However, if we want to flatten the spherical map further onto a rectangle, we need to interpolate the value of cortical thickness for each  $(\theta, \varphi)$ . However, the use of spherical harmonic expansion can avoid the interpolation problem. For this we need to discretize  $[0, \pi] \otimes (0, 2\pi]$  into finite number of pixels.

```
theta_d=0:0.01:pi;
varphi_d=0:0.01:2*pi;
m=length(theta_d);
n=length(varphi_d);
```

There will be total  $m \times n$  pixels in the flat map. Then for pixel value  $(\theta, \varphi)$ , we compute the basis  $Y_{lm}(\theta, \varphi)$  and plot it. Here we show how to flatten the basis  $Y_{3,1}$  and  $Y_{10,2}$  (Figure 11.12).

```
theta=kron(ones(1,n),theta_d');
theta=reshape(theta,1,m*n);
varphi=kron(ones(m,1),varphi_d);
varphi=reshape(varphi,1,m*n);

Ylm= Y_lm(3,1,theta,varphi);
square=reshape(Ylm,m,n);
figure;imagesc(square); colormap('hot'); colorbar
set(gcf,'Color','w')
```

**FIGURE 11.12**

Spherical harmonic basis  $Y_{3,1}$  and  $Y_{10,2}$  are mapped onto a rectangle easily by discretizing the spherical angles  $(\theta, \varphi)$ . Any linear combination of spherical harmonics can then be easily mapped onto the rectangle.

```

Ylm= Y_lm(10,2,theta,varphi);
square=reshape(Ylm,m,n);
figure;imagesc(square); colormap('hot'); colorbar
set(gcf,'Color','w')

```

The same idea can be used to flatten any linear combination of spherical harmonics. Therefore, once we have weighted-SPHARM representation of any measurements on the cortical surface, it can be easily mapped onto a rectangle. We have written this as a function **SPHARM2square**. It requires the estimated spherical harmonic coefficients **fourier.x** of cortical thickness (Figure 11.11).

```
square=SPHARM2square(fourier.x,42, 0.001);
```

## 11.6 Encoding Surface Asymmetry

Given the weighted spherical harmonic representation, we need to establish surface correspondence between hemispheres and between subjects. This requires establishing anatomical correspondence using *surface registration*. The main motivation for the surface registration is to establish proper alignment for cortical thickness to be compared across subjects and between hemispheres. Previously, the cortical surface registration was performed by minimizing an objective function that measures the global fit of two surfaces while maximizing the smoothness of the deformation in such a way that the sulcal and gyral

folding patterns are matched smoothly [363, 301, 76]. In the weighted spherical harmonic representation, surface registration is straightforward and does not require any sort of explicit time consuming optimization. Consider a surface  $\hat{h}_i$  obtained from coordinate functions  $v_i$  measured at points  $\Omega_1, \dots, \Omega_n$ :

$$\hat{h}_i(\Omega) = \sum_{l=0}^k \sum_{m=-l}^l e^{-l(l+1)\sigma} \langle v_i, Y_{lm} \rangle(\Omega).$$

Consider another surface  $\hat{j}_i$  obtained from coordinate functions  $w_i$  measured at points  $\Omega'_1, \dots, \Omega'_m$ :

$$\hat{j}_i(\Omega) = \sum_{l=0}^k \sum_{m=-l}^l e^{-l(l+1)\sigma} \langle w_i, Y_{lm} \rangle(\Omega).$$

Suppose the surface  $\hat{h}_i$  is deformed to  $\hat{h}_i + d_i$  under the influence of the displacement vector field  $d_i$ . We wish to find  $d_i$  that minimizes the discrepancy between  $\hat{h}_i + d_i$  and  $\hat{j}_i$  in the finite subspace  $\mathcal{H}_k$ . This can be easily done by noting that

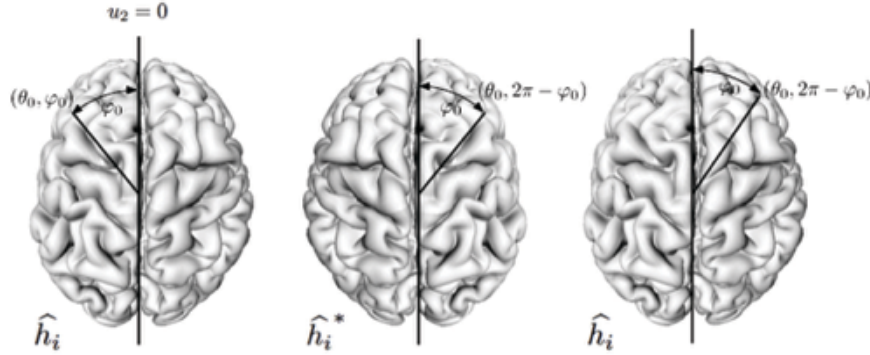
$$\sum_{l=0}^k \sum_{m=-l}^l e^{-l(l+1)\sigma} (w_{lm}^i - v_{lm}^i) Y_{lm}(\Omega) = \arg \min_{d_i \in \mathcal{H}_k} \left\| \hat{h}_i + d_i - \hat{j}_i \right\|. \quad (11.22)$$

The proof of this statement is given in [71]. This implies that the optimal displacement in the least squares sense is obtained by simply taking the difference between two weighted spherical harmonic representations and matching coefficients of the same degree and order. Then a specific point  $\hat{h}_i(\Omega_0)$  in one surface corresponds to  $\hat{j}_i(\Omega_0)$  in the other surface. We refer to this point-to-point surface correspondence as the *spherical harmonic correspondence*.

The spherical harmonic correspondence can be further used to establish the inter-hemispheric correspondence by letting  $\hat{j}_i$  be the mirror reflection of  $\hat{h}_i$ . The mirror reflection of  $\hat{h}_i$  with respect to the midsaggital cross section  $u_2 = 0$  is simply given by

$$\hat{j}_i(\theta, \varphi) = \hat{h}_i^*(\theta, \varphi) = \hat{h}_i(\theta, 2\pi - \varphi),$$

where  $*$  denotes the mirror reflection operation (Figure 11.13). The specific point  $\hat{h}_i(\theta_0, \varphi_0)$  in the left hemisphere will be mirror reflected to  $\hat{j}_i(\theta_0, 2\pi - \varphi_0)$  in the right hemisphere. The spherical harmonic correspondence of  $\hat{j}_i(\theta_0, 2\pi - \varphi_0)$  is  $\hat{h}_i(\theta_0, 2\pi - \varphi_0)$ . Hence, the point  $\hat{h}_i(\theta_0, \varphi_0)$  in the left hemisphere corresponds to the point  $\hat{h}_i(\theta_0, 2\pi - \varphi_0)$  in the right hemisphere. This establishes the inter-hemispheric anatomical correspondence. The schematic of obtaining this inter-hemispheric correspondence is given in Figure 11.13. This inter-hemispheric correspondence is used to compare cortical thickness

**FIGURE 11.13**

The point  $\hat{h}_i(\theta_0, \varphi_0)$  (left) corresponds to  $\hat{h}_i^*(\theta, 2\pi - \varphi_0)$  (middle) after mirror reflection with respect to the midsagittal cross section  $u_2 = 0$ . From the spherical harmonic correspondence,  $\hat{h}_i^*(\theta, 2\pi - \varphi_0)$  corresponds to  $\hat{h}_i(\theta, 2\pi - \varphi_0)$  (right). This establishes the mapping from the left hemisphere to the right hemisphere in least squares fashion.

measurements  $f$  across the hemispheres. The weighted spherical harmonic representation of cortical thickness  $f$  is

$$\hat{g}(\theta, \varphi) = \sum_{l=0}^k \sum_{m=-l}^l e^{-l(l+1)\sigma} \langle f, Y_{lm} \rangle Y_{lm}(\theta, \varphi).$$

At a given position  $\hat{h}_i(\theta_0, \varphi_0)$ , the corresponding cortical thickness is  $\hat{g}(\theta_0, \varphi_0)$ , which should be compared with the thickness  $\hat{g}(\theta_0, 2\pi - \varphi_0)$  at position  $\hat{h}_i(\theta_0, 2\pi - \varphi_0)$ :

$$\hat{g}(\theta_0, 2\pi - \varphi_0) = \sum_{l=0}^k \sum_{m=-l}^l e^{-l(l+1)\sigma} \langle f, Y_{lm} \rangle Y_{lm}(\theta_0, 2\pi - \varphi_0). \quad (11.23)$$

The equation (11.23) can be rewritten using the property of spherical harmonics:

$$\begin{aligned} Y_{lm}(\theta, 2\pi - \varphi) &= \begin{cases} -Y_{lm}(\theta, \varphi), & -l \leq m \leq -1, \\ Y_{lm}(\theta, \varphi), & 0 \leq m \leq l, \end{cases} \\ \hat{g}(\theta_0, 2\pi - \varphi_0) &= \sum_{l=0}^k \sum_{m=-l}^{-1} e^{-l(l+1)\sigma} \langle f, Y_{lm} \rangle Y_{lm}(\theta_0, \varphi_0) \\ &\quad - \sum_{l=0}^k \sum_{m=0}^l e^{-l(l+1)\sigma} \langle f, Y_{lm} \rangle Y_{lm}(\theta_0, \varphi_0). \end{aligned}$$

Comparing with the expansion for  $\widehat{g}(\theta_0, \varphi_0)$ , we see that the negative order terms are invariant while the positive order terms change sign. Hence we define the symmetry and asymmetry indices as follows.

**Definition 17** *The symmetry index is defined as*

$$\begin{aligned} S(\theta, \varphi) &= \frac{1}{2} [\widehat{g}(\theta, \varphi) + \widehat{g}(\theta, 2\pi - \varphi)] \\ &= \sum_{l=0}^k \sum_{m=-l}^{-1} e^{-l(l+1)\sigma} \langle f, Y_{lm} \rangle Y_{lm}(\theta_0, \varphi_0), \end{aligned}$$

while the asymmetry index is defined as

$$\begin{aligned} A(\theta, \varphi) &= \frac{1}{2} [\widehat{g}(\theta, \varphi) - \widehat{g}(\theta, 2\pi - \varphi)] \\ &= \sum_{l=0}^k \sum_{m=0}^l e^{-l(l+1)\sigma} \langle f, Y_{lm} \rangle Y_{lm}(\theta_0, \varphi_0). \end{aligned}$$

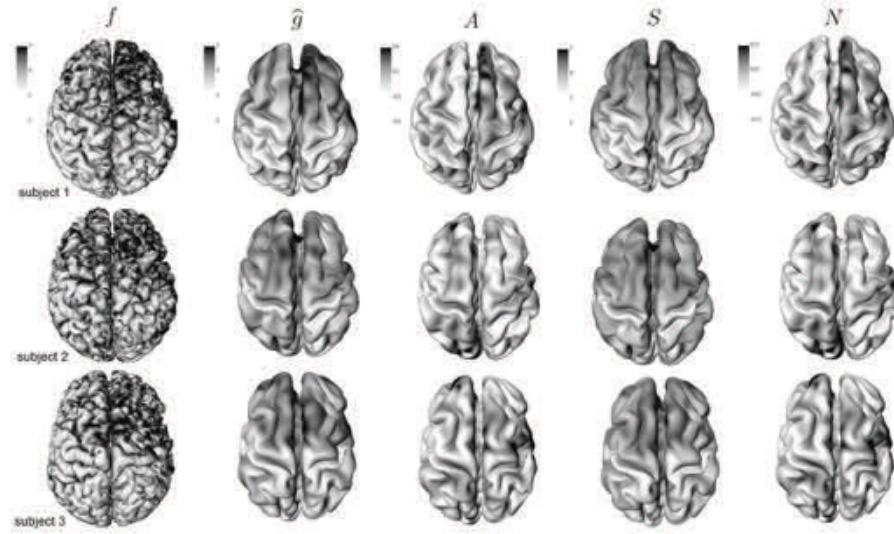
We normalize the asymmetry index by dividing it by the symmetry index as

$$\begin{aligned} N(\theta, \varphi) &= \frac{\widehat{g}(\theta, \varphi) - \widehat{g}(\theta, 2\pi - \varphi)}{\widehat{g}(\theta, \varphi) + \widehat{g}(\theta, 2\pi - \varphi)} \\ &= \frac{\sum_{l=1}^k \sum_{m=-l}^{-1} e^{-l(l+1)\sigma} \langle f, Y_{lm} \rangle Y_{lm}(\theta, \varphi)}{\sum_{l=0}^k \sum_{m=0}^l e^{-l(l+1)\sigma} \langle f, Y_{lm} \rangle Y_{lm}(\theta, \varphi)}. \end{aligned}$$

We refer to this index as the *normalized asymmetry index*. The numerator is the sum of all negative orders while the denominator is the sum of all positive and the 0-th orders. Note that  $N(\theta, 0) = N(\theta, \pi) = 0$ . This index is intuitively interpreted as the normalized difference between cortical thickness in the left and the right hemispheres. Note that the larger the value of the index, the larger the amount of asymmetry. The index is invariant under the affine scaling of the human brain so it is not necessary to control for the global brain size difference in the later statistical analysis. Figure 11.14 shows the asymmetry index for three subjects.

## 11.7 Case Study: Cortical Asymmetry Analysis

As an application of the weighted spherical harmonic representation, we show how to perform cortical asymmetry analysis.

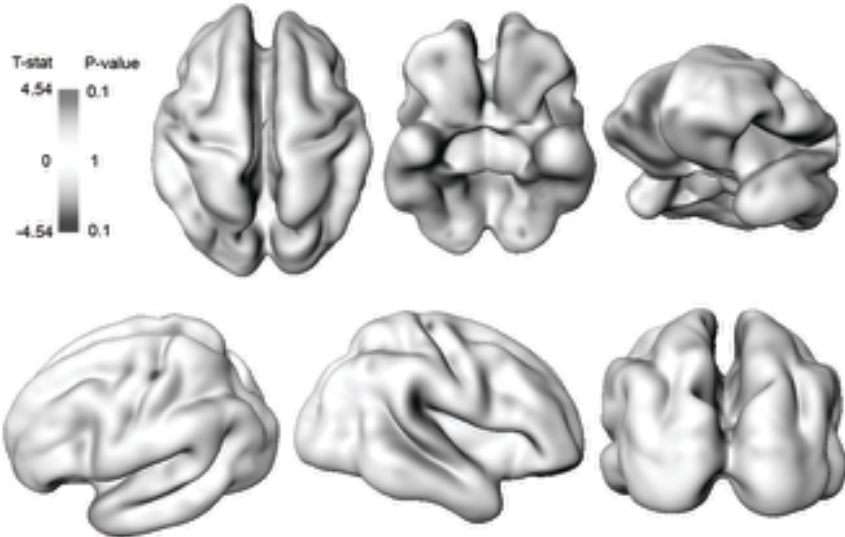
**FIGURE 11.14**

Three representative subjects showing cortical thickness ( $f$ ), its weighted-SPHARM representation ( $\hat{g}$ ), asymmetry index ( $A$ ), symmetry index ( $S$ ) and normalized asymmetry index ( $N$ ). The cortical thickness is projected onto the original brain surfaces while all other measurements are projected onto the 42-th degree weighed spherical harmonic representation.

### 11.7.1 Descriptions of Data Set

Three Tesla  $T_1$ -weighted MR scans were acquired for 16 high functioning autistic and 12 control right handed males. The data set is first published in [76] with the detailed descriptions. The autistic subjects were diagnosed by a trained and certified psychologist at the Waisman Center at the University of Wisconsin-Madison [98]. The average ages were  $17.1 \pm 2.8$  and  $16.1 \pm 4.5$  for control and autistic groups respectively. Image intensity nonuniformity was corrected using a nonparametric nonuniform intensity normalization method and then the image was spatially normalized into the Montreal neurological institute stereotaxic space using a global affine transformation [85]. Afterwards, an automatic tissue-segmentation algorithm based on a supervised artificial neural network classifier was used to segment gray and white matters.

Triangle meshes for outer cortical surfaces were obtained by a deformable surface algorithm [237] and the mesh vertex coordinates  $v_i$  were obtained. At each vertex, cortical thickness  $f$  was also measured. Once we obtained the outer cortical surfaces of 28 subjects, the weighted spherical harmonic representations  $\hat{h}_i$  were constructed. We used bandwidth  $\sigma = 0.001$  corresponding to  $k = 42$  degrees. The weighted spherical harmonic representations for three

**FIGURE 11.15**

The statistically significant regions of cortical asymmetry thresholded at the corrected P-value of 0.1. The P-value has been corrected for multiple comparisons.

representative subjects are given in Figure 11.14. The symmetry ( $S$ ), asymmetry ( $A$ ) and normalized asymmetry ( $N$ ) indices are computed. The normalized asymmetry index is used in localizing the regions of cortical asymmetry difference between the two groups. These indices are projected on the average cortical surface (Figure 11.14). The average cortical surface is constructed by averaging the Fourier coefficients of all subjects within the same spherical harmonics basis following the spherical harmonic correspondence. The average surface serves as an anatomical landmark for displaying these indices as well as for projecting the final statistical analysis results in the next section.

### 11.7.2 Statistical Inference on Surface Asymmetry

For each subject, the normalized asymmetry index  $A(\theta, \varphi)$  was computed and modeled as a Gaussian random field. The null hypothesis is that  $A(\theta, \varphi)$  is identical in the both groups for all  $(\theta, \varphi)$ , while the alternate hypothesis is that there is a specific point  $(\theta_0, \varphi_0)$  at which the normalized asymmetry index is different. The group difference on the normalized asymmetry index was tested using the  $T$  random field, denoted as  $T(\theta, \varphi)$ . Since we need to perform the test on every point on the cortical surface, it becomes a multiple comparison problem. We used the random field theory based  $t$  statistic thresholding

to determine statistical significance [394]. The probability of obtaining false positives for the one-sided alternate hypothesis is given by

$$P\left[\sup_{(\theta,\varphi)\in S^2} T(\theta,\varphi) > h\right] \approx \sum_{d=0}^2 R_d(S^2) \mu_d(h), \quad (11.24)$$

where  $R_d$  is the  $d$ -dimensional *Resel* of  $S^2$ , and  $\rho_d$  is the  $d$ -dimensional *Euler characteristic (EC) density* of the  $T$ -field [394, 396]. The Resels are

$$R_0(S^2) = 2, R_1(S^2) = 0, R_2(S^2) = \frac{4\pi}{\text{FWHM}^2},$$

where FWHM is the *full width at the half maximum* of the smoothing kernel. The FWHM of the heat kernel used in the weighted spherical harmonic representation is not given in a closed form, so it is computed numerically. From (11.6), the maximum of the heat kernel is obtained when  $\Omega \cdot \Omega' = 1$ . Then we numerically solve for  $\Omega \cdot \Omega'$ :

$$\frac{1}{2} \sum_{l=0}^k \frac{2l+1}{4\pi} e^{-l(l+1)\sigma} = \sum_{l=0}^k \frac{2l+1}{4\pi} e^{-l(l+1)\sigma} P_l^0(\Omega \cdot \Omega').$$

In previous surface data smoothing techniques [83, 76], a FWHM of between 20 to 30 mm was used for smoothing data directly along the brain surface. In our study, we used a substantially smaller FWHM since the analysis is performed on the unit sphere, which has a smaller surface area. The compatible Resels of the unit sphere can be obtained by using the bandwidth of  $\sigma = 0.001$ , which corresponds to a FWHM of 0.0968 mm. Then, based on the formula (11.24), we computed the multiple-comparison-corrected P-value and thresholded at  $\alpha = 0.1$  (Figure 11.15). We found that the central sulci and the prefrontal cortex exhibit abnormal cortical asymmetry pattern in autistic subjects. The larger positive  $t$  statistic value indicates thicker cortical thickness with respect to the corresponding thickness at the opposite hemisphere.

## 11.8 Discussion

We have presented a novel cortical asymmetry technique called the weighted spherical harmonic representation that unifies surface representation, parameterization, smoothing, and registration in a unified mathematical framework. The weighed spherical representation is formulated as the least squares approximation to an isotropic heat diffusion on a unit sphere in such a way that the physical time of heat diffusion controls the amount of smoothing in the weighted spherical harmonic representation. The methodology is used in

modeling cortical surface shape asymmetry. Within this framework the asymmetry index, that measures the amount of asymmetry presented in the cortical surface, was constructed as the ratio of the weighted spherical harmonic representation of negative and positive orders. The regions of the statistically different asymmetry index are localized using random field theory. As an illustration, the methodology was applied quantifying the abnormal cortical asymmetry pattern of autistic subjects. The weighted spherical harmonic representation is a very general surface shape representation so it can be used for any type of surface objects that are topologically equivalent to a unit sphere.

